NASA CONTRACTOR REPORT

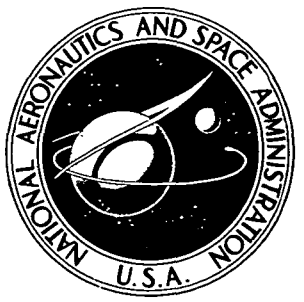

NASA CR-2387

NASA CR-2387

ON THE THEORY OF COMPLIANT WALL DRAG REDUCTION IN TURBULENT BOUNDARY LAYERS

by Robert L. Ash

Prepared by
OLD DOMINION UNIVERSITY
Norfolk, Va. 23508
for Langley Research Center

NATIONAL AERONAUTICS AND SPACE ADMINISTRATION • WASHINGTON, D. C. • APRIL 1974

1. Report No.	2. Government Accession No.	3. Recipient's Catalog No.
NASA CR-2387		

4. Title and Subtitle	5. Report Date
ON THE THEORY OF COMPLIANT WALL DRAG REDUCTION IN TURBULENT BOUNDARY LAYERS.	April 1974
	6. Performing Organization Code

7. Author(s)	8. Performing Organization Report No.
ROBERT L. ASH	Technical Report 73-T8
	10. Work Unit No. 501-06-08-01

9. Performing Organization Name and Address	11. Contract or Grant No.
Old Dominion University School of Engineering Norfolk, Virginia	NAS1-11707
	13. Type of Report and Period Covered Contractor Report

12. Sponsoring Agency Name and Address	14. Sponsoring Agency Code
National Aeronautics and Space Administration Washington, D. C. 20546	

15. Supplementary Notes

FINAL REPORT

16. Abstract

A theoretical model has been developed which can explain how the motion of a compliant wall reduces turbulent skin friction drag. Available experimental evidence at low speeds has been used to infer that a compliant surface selectively removes energy from the upper frequency range of the energy containing eddies and through resulting surface motions can produce locally negative Reynolds stresses at the wall. The theory establishes a preliminary amplitude and frequency criterion as the basis for designing effective drag reducing compliant surfaces.

17. Key Words (Suggested by Author(s))	18. Distribution Statement
Drag reduction Turbulent boundary layer Compliant wall	Unclassified - Unlimited

19. Security Classif. (of this report)	20. Security Classif. (of this page)	21. No. of Pages	22. Price*
Unclassified	Unclassified	43	$3.25

*For sale by the National Technical Information Service, Springfield, Virginia 22151

Page Intentionally Left Blank

CONTENTS

FIGURES

TABLE

ON THE THEORY OF COMPLIANT WALL DRAG REDUCTION IN TURBULENT BOUNDARY LAYERS

by Robert L. Ash[1]

SUMMARY

A theoretical model has been developed which can explain how the motion of a compliant wall reduces skin friction drag. The experiments reported by Blick, et al. (Ref. 1) and Mattout (Ref. 2) have been used to infer that a compliant surface selectively removes energy from the upper frequency range of the energy containing turbulent eddies and through resulting surface motions can produce locally negative Reynolds stresses at the wall. The theory establishes a preliminary amplitude and frequency criterion as the basis for designing effective drag reducing compliant surfaces.

INTRODUCTION

M. O. Kramer (Refs. 3 and 4) has been credited with the original idea of drag reduction by a flexible or compliant surface. His early experiments with submerged flexible rubber cylinders indicated potential drag reductions of 50 percent. However, his experiments were not closely controlled (drag was measured on cylinders towed behind an outboard motor boat) and no one has been able to duplicate his experimental results. Kramer suggested that the mechanism responsible for drag reduction was a delay in the transition from a laminar boundary layer to a turbulent boundary layer. Theoretical models proposed by Benjamin (Refs. 5-7), Kaplan (Ref. 8), Landahl (Ref. 9), Nonweiler (Ref. 10) and Gyorgyfalvy (Ref. 11) all have indicated it is possible to stabilize a laminar boundary layer with appropriate flexible wall materials. However, numerous experiments with compliant wall models in water and air flows have produced no conclusive data showing a drag reduction due to transition delay (See Refs. 12-14, for example).

---

[1]Associate Professor of Engineering, School of Engineering, Old Dominion University, Norfolk, Virginia 23508.

Aside from the transition delay, Kaplan (Ref. 8) and Gyorgyfalvy (Ref. 11) have indicated it is theoretically possible to produce some drag reduction by expanding the region of the transition boundary layer. That is, even though a compliant wall may in fact cause a laminar boundary layer to become unstable sooner (farther upstream), the rate of amplification of local fluctuations may be lower, causing the fully turbulent boundary layer to develop more slowly. Experiments by Karplus (Ref. 15) have shown that simultaneous early instability and arrested turbulent development can occur on some flexible surfaces.

At the present time, serious questions exist concerning whether any real material can be employed to either delay transition or retard the development of a fully turbulent boundary layer in a manner which can significantly reduce the skin friction drag. Hence, the present state appears to be one in which theory predicts significant drag reduction, while experiments show no drag reduction. On the other hand, experiments with fully turbulent boundary layers have been more encouraging.

In 1966, Fisher and Blick (Ref. 16) reported on preliminary experiments with low speed turbulent air boundary layers over flexible membrance surfaces. Their experiments indicated a skin friction drag reduction of nearly 50 percent was possible under some conditions. Since that time, Blick and his coworkers at the University of Oklahoma have presented substantial evidence (Refs. 17-22) to indicate that significant drag reduction is indeed possible. However, their experiments were not closely controlled and to date no one has isolated the design parameters required to produce such large drag reductions in other experiments. A more modest drag reduction of 10 percent has been reported by Lissaman and Harris (Ref. 23) with essentially the same type experimental apparatus as Blick although stringers were used to prevent large amplitude panel flutter.

The purpose of the present report is to explain a preliminary theoretical model of how a flexible wall can interact with a fully turbulent boundary layer to reduce skin friction drag. Theoretical studies of the turbulent boundary layer-compliant wall interaction have been reported by Ffowcs-Williams (Ref. 24), Blick (Ref. 25) and Semenov (Ref. 26). However, none of the three have isolated the design parameters sufficiently to allow testing of their theories. The present model has attempted to concentrate on identifying the important design parameters without fully exploring the mathematical solutions. A more complete mathematical model will be the subject of a future report.

At the present time, only the uncoupled fluid and solid equations of motion have been investigated. Moreover, the investigation has concentrated primarily on the equations governing the wall motion even though most of the previous literature has concentrated on the turbulent boundary layer model. The basis for this change in approach is the fact that the compliancy parameters used in the uncoupled fluid flow models have been unable to isolate the material design parameters needed to select a drag reducing compliant material. In addition, because of the success of Blick and his coworkers with membrane surfaces, primary attention has been given to the analysis of a rectangular membrane.

Ultimately, the turbulent boundary layer equations must be coupled with the equations governing the surface motion in order to completely understand the fluid-wall interaction. However, the characteristics of a surface motion which can potentially produce a drag reduction have not been identified at this time. The simple phase lag model used so heavily by previous investigators (Ref. 5-11 and 24-26) appears inadequate due to the random nature of an actual turbulent wall pressure fluctuation as well as the uncertainty in whether drag reduction is caused by a local wall motion due to a local pressure fluctuation or by wall motions driven by pressure fluctuations acting some distance away from regions where a drag reduction occurs.

During the preliminary phases of this study, an attempt was made to develop general analytic solutions for membrane and elastic slab surface motions when subjected to an arbitrarily varying local surface pressure. Solutions have been developed for a rectangular membrane surface subjected to nonuniform tension loads (Appendix A) and for a two dimensional elastic slab material subjected to a sinusoidally varying surface pressure (Appendix B). The elastic slab solution is not original, and is based on the solution presented by Nonweiler (Ref. 10). Both solutions allow frequency response analyses, but the membrane solution is unjustifiably complicated and the elastic slab solution is too restricted to permit detailed studies of the interaction between a compliant wall and a turbulent boundary layer.

The present report will concentrate on the compliant wall effect over membrane surfaces since they are the only ones which have shown large experimentally documented drag reductions.

MOTION OF A RANDOMLY EXCITED, NONUNIFORMLY LOADED MEMBRANE

Using the experiments of Blick and his coworkers as a guide, it can be justifiably argued that variations in membrane tension in the direction of flow due to the local drag force are negligibly small compared to the applied edge tensions. An attempt was made to use the variable tension solution reported in Appendix A but was abandoned because the dimensionless drag force parameter based on Blick's experiments was so small, the only way eigenvalues could be calculated was by approximating the Bessel functions with the same trigonometric functions that result when the drag force was neglected. As a consequence, the appropriate equation governing the motion of a rectangular membrane subjected to different (but constant) tensions in the x- and y-directions was:

$$T_x \frac{\partial \bar{z}}{\partial \bar{x}} + T_y \frac{\partial \bar{z}}{\partial \bar{y}} + \bar{p}(\bar{x},\bar{y},\bar{t}) = \rho h \frac{\partial^2 \bar{z}}{\partial \bar{t}^2} \quad , \tag{1}$$

where T_x is the tension applied in x- or flow-direction and T_y is the tension applied in the y- or transverse-direction (N/m). The local instantaneous pressure is $\bar{p}$ and ρ and h are the membrane density and thickness, respectively. For simplicity, it was assumed that the membrane was initially flat and motionless. As a result, the initial conditions were:

$$\bar{z}(\bar{x},\bar{y},o) = \frac{\partial \bar{z}}{\partial \bar{t}} (\bar{x},\bar{y},o) = 0. \tag{2}$$

Since the edges of the membrane were anchored, the appropriate boundary conditions were:

$$\bar{z}(o,\bar{y},\bar{t},) = \bar{z}(L,\bar{y},\bar{t}) = \bar{z}(\bar{x},o,\bar{t}) = \bar{z}(\bar{x},\bar{W},\bar{t}) = 0, \tag{3}$$

where L was the membrane length in the direction of flow and W was the membrane width. If dimensionless variables x,y,z,t and p are defined by:

$$x = \frac{\bar{x}}{L} \ , \ y = \frac{\bar{y}}{L} \left(T_x/T_y\right)^{\frac{1}{2}}, \ z = \frac{\bar{z}}{L} \ , \ t = \frac{\bar{t}}{h} \left(T_x/\rho h\right)^{\frac{1}{2}} \ ,$$

and $$p = L^2\bar{p}/(hT_x),$$

the resulting dimensionless form of equation (1) is:

$$\nabla^2 z + p(x,y,t,) = \frac{\partial^2 z}{\partial t^2} , \tag{4}$$

where

$$\nabla^2 = \frac{\partial^2}{\partial x^2} + \frac{\partial^2}{\partial y^2} .$$

The initial conditions have exactly the same form as conditions (2) and the boundary conditions become:

$$z(o,y,t,) = z(1,y,t) = z(x,o,t) = z(x,\beta,t) = 0 \tag{5}$$

where

$$\beta = \frac{W}{L} (Tx/Ty)^{\frac{1}{2}} . \tag{6}$$

Assuming the turbulent wall pressure has a Laplace transformation, a double Fourier transform and a Laplace transformation can be employed on equation (4), subjected to (2) and (5) to yield

$$\phi_{mn} = \left[s^2 + \left(\frac{m\pi}{\beta}\right)^2 + (n\pi)^2 \right] \zeta_{mn} \tag{7}$$

where

$$\phi_{mn} = \int_0^\beta \int_0^1 \int_0^\infty p(x,y,t) e^{-st} \sin n\pi x \sin \frac{m\pi y}{\beta} \, dt dx dy \tag{8}$$

and

$$\zeta_{mn} = \int_0^\beta \int_0^1 \int_0^\infty z(x,y,t) e^{-st} \sin n\pi x \sin \frac{m\pi y}{\beta} \, dt dx dy \tag{9}$$

If the wall pressure function is known, equation (7) yields a solution for ζ_{mn} which can be inverted to find z. Specifically,

$$z(x,y,t) = \frac{\Delta}{\beta} \sum_{n=1} \sum_{m=1} L^{-1} \left\{ \frac{\phi_{mn}}{s^2 + \left(\frac{m\pi}{\beta}\right)^2 + (n\pi)^2} \right\} \sin \frac{m\pi y}{\beta} \sin n\pi x \tag{10}$$

where L^{-1} { } is the inverse Laplace transformation.

Because no damping has been included in the governing equation (4), the solution will predict sharp resonant peaks when the local pressure $p(x,y,t)$ has a frequency component given by $\sin \gamma_{mn} \pi t$, where

$$\gamma_{mn} = \left[\left(\frac{m}{\beta}\right)^2 + n^2\right]^{\frac{1}{2}} \tag{11}$$

However, the predicted resonance amplitudes are of secondary interest here since the actual fluid damping has been omitted from this analysis. It is more important to realize that inversion of equation (10) will generally yield a solution in the form:

$$z(x,y,t) = \sum_{n=1}^{\infty} \sum_{m=1}^{\infty} A_{mn} \sin n\pi x \sin \frac{m\pi y}{\beta} \sin \gamma_{mn} t. \tag{12}$$

This suggests that there will be a band of frequencies (determined by the γ_{mn}) over which the membrane will exhibit preferential response. This "filter" idea is discussed by Vaicaitis (Ref. 27) in his analysis of the response of structual panels when exposed to turbulent boundary layers. However, in his case of metal panels, the amplitude and frequency response apparently do not alter appreciably the structure of the turbulent boundary layer.

If the pressure field is approximated by a collection of randomly varying and randomly distributed pressure pulses, each pulse could be written in the form

$$p_i(x,y,t) = P_I \, \delta(x-x_o) \, \delta(y-y_o) \, \delta(t-t_o) \tag{13}$$

and the response to a single pressure pulse would be given by:

$$z_i(x,y,t) = \frac{4P_I}{\pi\beta} \sum_{n,m} \frac{1}{\gamma_{mn}} \sin \frac{m\pi y_o}{\beta} \sin n\pi x_o \sin \frac{n\pi y}{\beta} \sin n\pi x \sin \gamma_{mn}\pi(t-t_o), \tag{14}$$

$$t > t_o \quad .$$

Because γ_{mn} appears in the denominator, the above solution indicates a preference for membrane vibration frequencies near its fundamental vibration mode. The idea of a preferential response will be employed in the later analysis.

Walters (Ref. 28) measured the kinetic energy power spectra exhibited by a turbulent boundary layer over a rigid surface and over a compliant surface. The compliant surface was a 0.0254 mm thick polyvinyl-chloride (PVC) skin 3.66 m long and 0.61 m wide backed by a 0.76 cm thick polyurethane foam with a nominal porosity of 1.6 pores per mm (40 pores per inch--designated 40 PPI). The flow velocity was 15.25 m/sec. and the artifically tripped turbulent boundary layer was approximately 7.6 cm thick. In the vicinity of the wall ($y/\delta = 0.0033$), he observed the changes in power spectrum over a compliant wall shown in Figure 1. According to the data, both the high frequency and low frequency turbulent energy content have decreased over the compliant surface when compared with the rigid wall power spectrum. Simultaneously, the energy contained in the interval between 4 and 80 Hz($0.1 \leq k \leq 20$) has increased. The energy changes can be accounted for by the filter effect discussed by Vaicaitis.

In order to expand the concept of a filter effect, the characteristic membrane vibration frequencies must be determined for Walters' experiment. Since he did not measure the applied tension loads, they must be estimated. Using Blick's earlier experiments (Ref. 1) as a guide, tensions applied in the x- or flow-direction on a much smaller membrane varied between 1.9 and 120 N/m, while tensions in the y-direction varied between 1.9 and 56 N/m. If the tension in the x-direction was 7 N/m (corresponding to an applied force of 1.3 N) and the tension in the y-direction was 0.35 N/m (corresponding to applied force of 1.3 N), β from equation (11) would be 0.745, and the first vibration mode for the membrane would be 3.4 Hz. These tensions appear reasonable since Blick in his previous work used a PVC skin which was 2.5 times thicker than Walters', and furthermore Walters' discussion appears to indicate that the membrane was loosely attached and tension was produced by thermal shrinkage resulting from an 8°C reduction in temperature.

Since the first fundamental vibration mode was approximately 4 Hz, any pressure fluctuation which had primary frequencies above 4 Hz and less than a few hundred Hz could be accomodated readily by the membrane. This accomodation could conceivably reduce the turbulent streak shedding intensity (Ref. 29) caused by eddies in that frequency range while simultaneously preserving eddies with those frequencies. However as the frequency increased, the pressure fluctuation was associated with eddies of decreasing size and the surface area

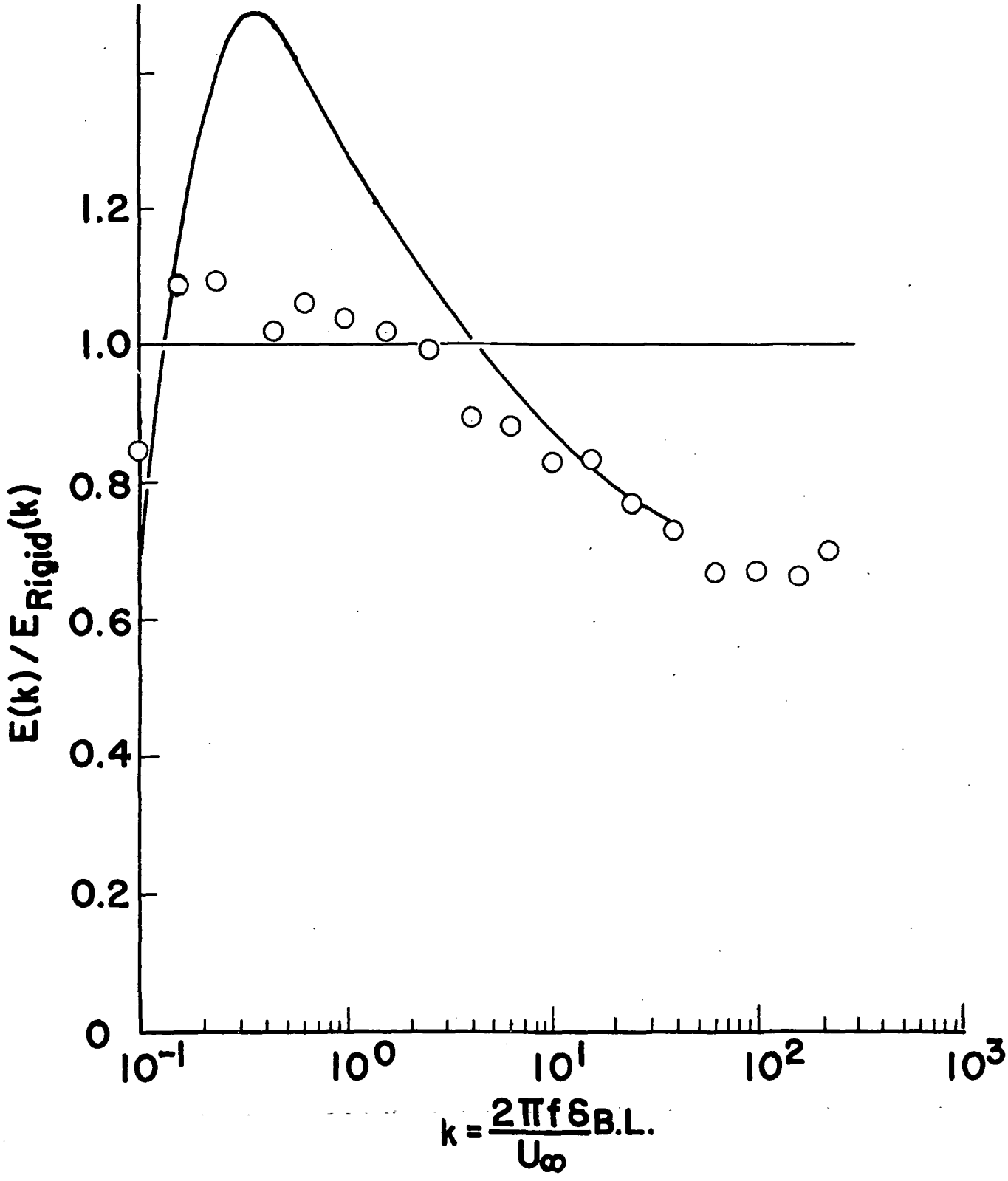

Figure 1.- Effect of a vibrating membrane on the turbulent energy spectrum. From Walters (ref. 28).

affected by the high frequency fluctuations associated with the particular eddy would become small. As the characteristic frequency increased and the area decreased, the local pressure fluctuations should be well approximated by pulses of the type given by equation (13). These high frequency, pulse-like disturbances could then result in a frequency exchange whereby some of the energy is extracted from the eddies and is ultimately fed back to the turbulent boundary layer at the lower frequencies which characterize the membrane vibration. Examination of the spectral data indicates that maximum energy removal has occurred in the high frequency portion of the energy containing eddies. The simultaneous increase in energy between 4 and 80 Hz may be accounted for by the excited membrane burst production and by preservation of existing eddies. For characteristic frequencies below 4 Hz, the eddies are expected to be quite large and the membrane should perceive a quasi-steady applied force, which make it less prone to vibrate and more likely to simply deflect.

To further expand this idea, the membrane should be easily excited over the band of frequencies in Figure 1 which show an increase in energy. In addition, higher frequency pressure fluctuations occurring at the membrane surface should behave like pressure pulses and can give up energy which is translated by the membrane into lower frequency surface motions. These lower frequency motions are communicated throughout the membrane. At the same time, they are dissipated by viscous interactions between the membrane and the turbulent boundary layer, as well as any interactions between the membrane and its substrate. The two dissipation mechanisms will be discussed separately. Because of dissipation, a continuous supply of energy will be withdrawn from the high frequency fluctuations and fed back to the turbulent boundary layer with frequencies which characterize the vibrating membrane.

MEMBRANE DAMPING BY THE TURBULENT BOUNDARY LAYER AND SIMULTANEOUS REDUCTION IN THE REYNOLDS STRESSES

In order to understand the membrane-wall flow region interaction, a brief discussion of the rigid wall-turbulent boundary layer interface is needed. Based on the fundamental research of Kline, Reynolds, Schraub and Runstadler (Ref. 29) at Stanford, the structure of a turbulent boundary layer near a wall is characterized by alternating streaks of low and high velocity flow as shown

in Figure 2. Kim, Kline and Reynolds (Ref. 30) have shown that Reynolds stresses and turbulent energy production occur primarily during periods of "bursting" in which segments of the low speed streaks are ejected up into the high velocity region. It is important to note that these ejected streaks then have a positive vertical or v' velocity fluctuation and because of their low speed, they simultaneously create a negative longitudinal or u' velocity fluctuation which makes a positive contribution to the Reynolds stress and therefore to turbulent energy production. The instability responsible for the onset of a burst was not described. However, at virtually the same time, Grass (Ref. 31) observed in the study of flow over smooth and rough surfaces that an inrush phase was an equally important part of the bursting process. He found that a high velocity inflow from the outer regions of the boundary layer immediately preceded the ejection of a low speed filament. Furthermore, his measurements indicated that this portion of the bursting process was of nearly the same importance as the actual ejection in the overall production of Reynolds stresses and turbulent kinetic energy. The inrush portion of the bursting process can be characterized by a negative v' fluctuation due to an arriving eddy and a positive u' fluctuation caused by the high velocity entrant fluid and dictated by conservation of mass--again making a positive contribution to the Reynolds stress. A simplified sketch of the activity associated with a single burst is shown in Figure 2.

As long as the amplitude of the membrane oscillations is not large (z_{max} should be less than the sublayer thickness to prevent roughness effects) the smooth wall streak shedding process for turbulence generation should continue to exist (in fact, Grass has shown that it exists even in flow over rough surfaces). However, an additional shedding mechanism is available and two negative Reynolds stress contributions are possible. If a high frequency pressure fluctuation initiates a membrane disturbance, low frequency waves will be propagated away from that disturbance through the membrane. As those wave motions propagate into regions where the fluid flow filaments are attached to the wall, bursting may not occur and the flow field shown in Figure 3 should exist. Under these conditions, values of the product u'v' would tend to be positive and the Reynolds stress would be negative. Furthermore, when a burst is initiated, the vibrating surface may be less selective in ejecting high or low velocity streaks. Grass has reported that the ejection of high speed

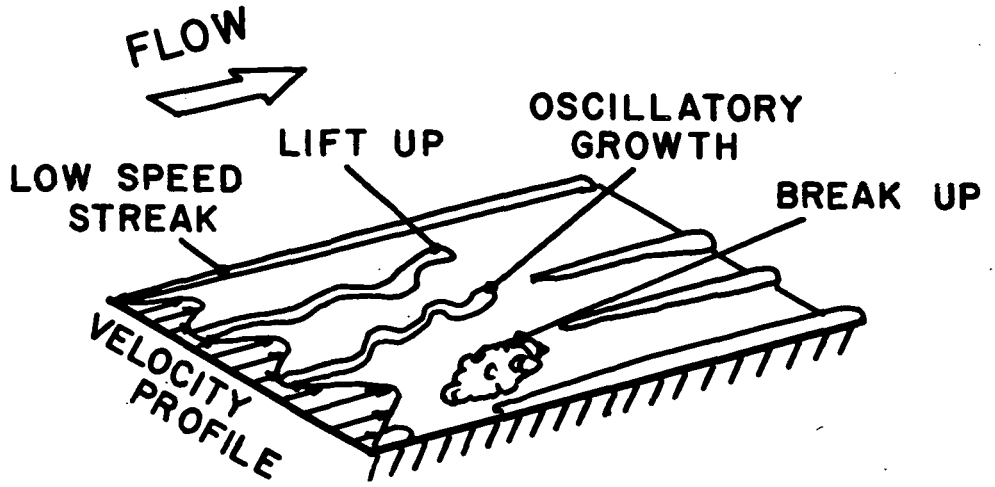

Figure 2a. Low speed streak pattern, showing various stages of development.

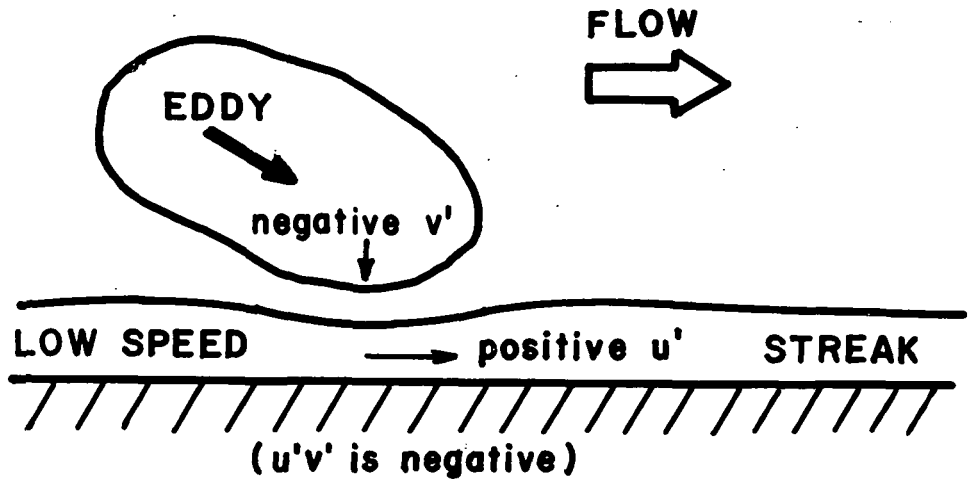

Figure 2b. Interaction between an eddy and a low speed streak along a rigid wall.

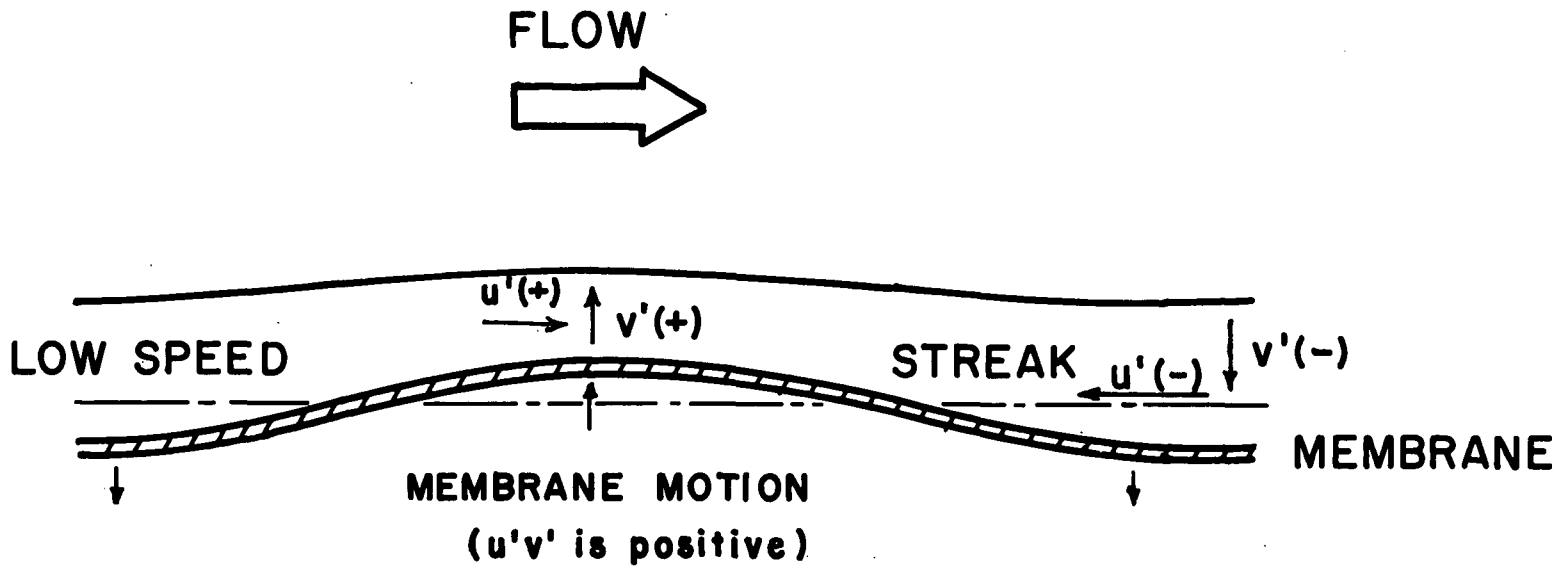

Figure 3. Interaction between a low speed streak and a vibrating membrane.

velocity streaks results in a negative Reynolds stress contribution. On the other hand, ejected low velocity streaks will still make positive contributions to the Reynolds stress, and the rigid wall turbulent generation mechanisms will remain, but the spectrum will be altered due to the ability of the wall to respond to eddies with characteristic frequencies near the vibration frequencies of the membrane and to its ability to selectively eject streaks.

The membrane motion and additional streak shedding mechanism does require energy, and it is proposed that this energy is withdrawn from the small, high frequency eddies and is converted to low frequency surface motions which are ultimately dissipated by interaction with the wall flow region. It would also be expected that the energy contained by the very large, low frequency eddies would decrease because there is a tendency for the low speed streaks to be broken up more rapidly due to the additional ejection mechanism. A corresponding reduction in power spectrum is shown in Figure 1. This single data point may be questioned, but Walters' experiments showed a persistant decrease in low frequency energy as his spectra were measured farther away from the wall.

THE ROLE OF BACKING MATERIALS IN COMPLIANT DRAG REDUCTION

One reason for the difficulty in achieving consistent drag reduction data can be attributed to effects caused by the backing material. If the previous explanation for compliant drag reduction in a turbulent boundary layer is correct, then the primary function of the backing material must be to control the amplitude of membrane oscillations. Compliant drag reduction can be described by the present theory as a controlled panel flutter phenomenon. The membrane must oscillate, but the amplitude must be low enough to maintain the "streaky" character of the wall flow regime with minimal increases in low speed streak ejection (i.e. without introducing roughness). If the backing material is fairly rigid, the membrane will oscillate at a very low amplitude. Obviously, the membrane cannot be attached to the backing material if membrane motions are the source of drag reduction. Furthermore, any gap between the membrane and the backing material will be the dominant parameter in controlling the maximum amplitude of the membrane oscillations.

In support of the contention that drag reduction was caused by controlled amplitude membrane motions and not by elastic substrate motions, the experiments of Walters (Ref. 28) shed further insight. He reported that when the membrane surface was bonded to the polyurethane substrate no drag reduction occurred. Furthermore, drag reduction did occur when the surface was not attached to the substrate. These observations suggest the backing material may have effectively prevented large amplitude panel flutter (which should be controlled in both cases) but it interfered with the frequency response of the surface.

DISCUSSION

Several points can be made concerning the reported successful drag reduction experiments which tend to support the proposed theory. First of all, from Walters' measurements the primary membrane vibration frequencies were located in the energy containing range of the turbulent boundary layer power spectrum. The energy containing range is generally considered to include all frequencies below ω_c (radians/sec.) (Ref. 32) given by:

$$k_c = \frac{\omega_c \delta_{B.L.}}{U_\infty} \cong 10 \tag{15}$$

where k_c is the critical wave number, U_∞ is the free stream velocity and $\delta_{B.L.}$ is the boundary layer thickness. Hence, Walters' fundamental membrane vibration modes were in the energy containing band. Apparently, only under these conditions can a membrane affect the Reynolds stresses significantly. It is also significant that Figure 1 indicates a withdrawal of energy from the high frequency end of the energy containing eddies as was already mentioned. These two ideas are consistent, since energy is required to drive the membrane and little energy is available at higher frequencies.

The present theory further suggests that there should be an optimum vibration frequency band which characterizes maximum compliant drag reduction. In order to determine whether such an optimum frequency range exists, the data compiled by Blick et al. (Refs. 1 and 19) in air and Mattout (Ref. 2) in water have been examined to see if a correlation existed between the drag reduction and the first fundamental membrane vibration mode. That is, the

vibration frequency should have been some fraction of the turbulent peak power frequency. Employing equation (14), the fundamental membrane vibration frequency is given by:

$$f_1 = \frac{1}{2}\left[\frac{T_y/w^2 + T_x/L^2}{\rho h}\right]^{\frac{1}{2}} \tag{16}$$

The nominal peak frequency in the turbulent boundary layer pressure as suggested by Bradshaw (Ref. 32) and observed by Bull (Ref. 33) is

$$f_{peak} = \frac{U_\infty}{2\pi\delta_{B.L.}} \tag{17}$$

The correlation of drag reduction with frequency ratio is shown in Figure 4. Due to the scatter, an optimum frequency is difficult to estimate (or refute). However, minimum skin friction drag appears to occur when the fundamental vibration frequency is approximately half the nominal peak power frequency. Much of the scatter can be attributed either directly to roughness effects or indirectly to roughness through the magnitude of the vibration amplitudes achieved by the membrane. In addition to roughness due to large amplitude motions, the amplitude may also have been too low in some cases to achieve appreciable wall-fluid interaction.

It has been the author's experience that roughness effects can hide this compliant effect. Roughness can be directly produced by variations in the membrane surface as well as nonhomogeneity and thickness variations in the substrate. It would appear that Blick's dry 25 PPI data shown in Figure 4 have resulted from a roughness dominated interaction. An optimum vibration amplitude must surely exist for the compliancy effect as well as the previously suggested optimum frequency. Variations in vibration amplitude could spread the data similar to that shown in Figure 4. Specifically, if the amplitude was too large, a roughness dominated interaction would occur, while too small amplitudes would result in no interactions.

An optimum amplitude can be further implied from some of the previously reported experiments. Blick et al. (Ref. 1) reported on one set of tests which were performed with constant membrane tensions over three different polyurethane foams. The foams were tested under dry conditions and when saturated with water.

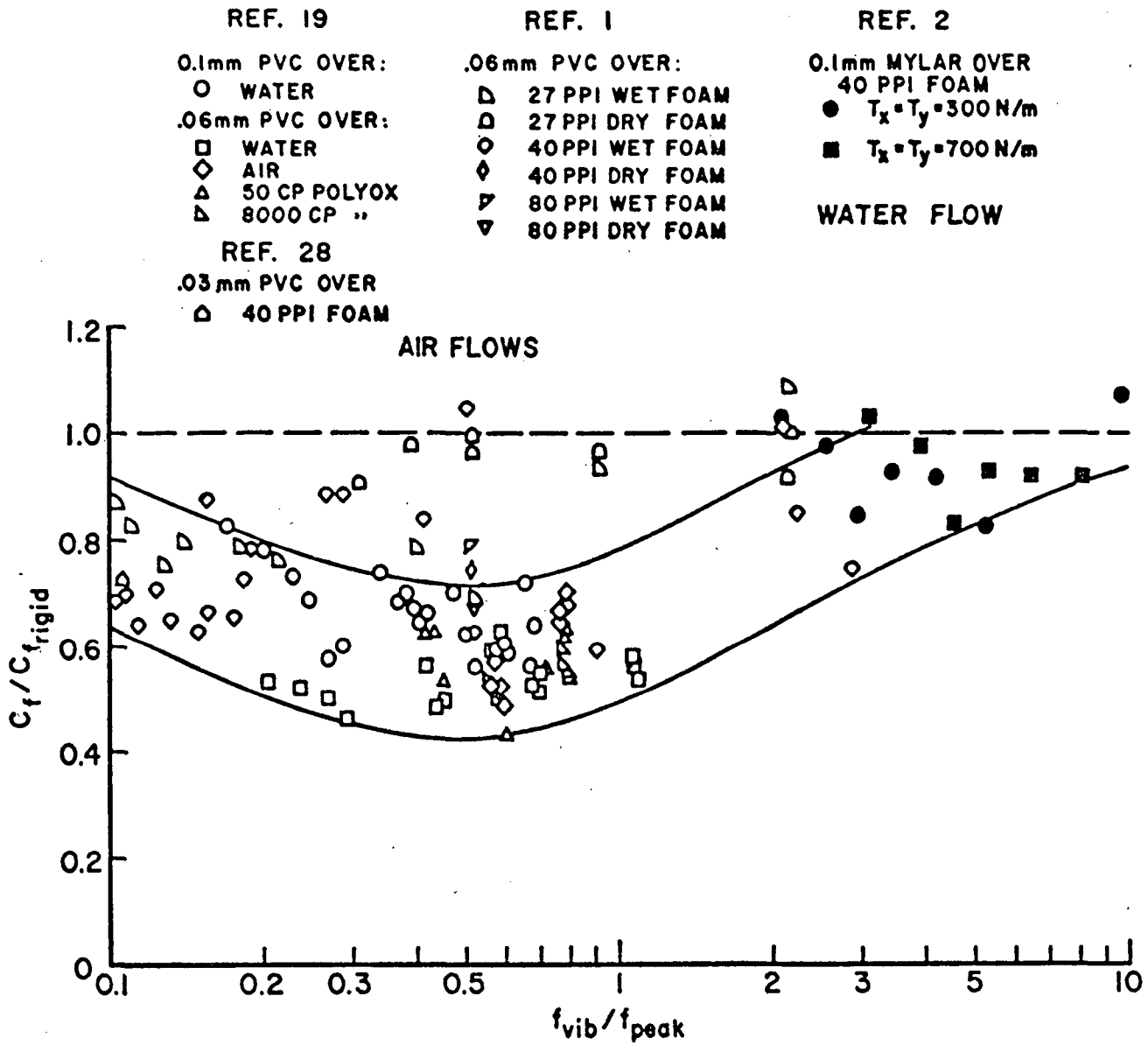

Figure 4. Compilation of experimental data showing influence of fundamental membrane vibration mode on skin friction coefficient.

A pseudo modulus of elasticity was measured by measuring the deflection of a weight supported by the different foam specimens. A compilation of the foam thickness and deformation moduli are given in Table 1. Because the foams were of the same polyurethane material, the true modulus of elasticity of each foam should have been linearly related (at least approximately) to the pseudo modulus measured by Blick. Furthermore, if each foam was in contact with the membrane surface, the amplitude of its oscillations was directly proportional to the substrate thickness and inversely proportional to the deformation modulus. Hence, the membrane amplitude should vary with the deformation parameter $\Delta\bar{a}$ given by

$$\Delta\bar{a} = \frac{T_s}{E_B} \tag{18}$$

where T_s is the substrate thickness and E_B is Blick's deformation modulus. Large values of $\Delta\bar{a}$ indicate large amplitude oscillations while small values indicate small amplitudes.

Before utilizing the amplitude parameter, its severe limitations must be emphasized. First of all, it represents a steady-state amplitude estimate, rather than a dynamic amplitude estimate. However, since all of the foams were made of polyurethane, they should show the same type of frequency dependence. Secondly, the water saturated foam is an entirely different structural material. The vibration amplitude of the water saturated foam most surely exhibits different frequency dependence than does the dry foam. Finally, if a gap was present between the membrane and the foam, it would dominate the amplitude of vibration. However, because of a general lack of controlled test data, it has been necessary to assume that the water saturated and dry foams exhibit similar frequency dependent amplitude responses, and that they were in good contact with the membrane surface. A plot of drag reduction as a function of amplitude parameter is shown in Figure 5.

As previously mentioned, the 25 PPI dry foam appears to be roughness dominated. Furthermore, the composite data plot in Figure 4 indicates a potential drag reduction of 57% when the fundamental vibration mode is 52% of the peak frequency in the turbulent power spectrum. Omitting the 25 PPI data point and assuming the trends indicated by the composite data are correct, the curve connecting the data points in Figure 5 can be drawn.

TABLE 1

CHARACTERISTIC PROPERTIES OF POLYURETHANE FOAMS
TESTED BY BLICK et al. (Ref. 1)

Type	Porosity (pores/mm)	Thickness (cm)	E_B (N/cm^2)	
			Dry	Water/Saturated
27 PPI	1.1	2.5	2.6	1.1
40 PPI	1.6	0.4	0.67	0.56
80 PPI	3.2	2.4	1.7	0.82

As has previously been mentioned, a gap may have been present between the PVC skin and the foam used in Walters' experiments. In the absence of a gap, the deformation of the foam substrate can be estimated and that estimate indicates very small amplitudes. The modulus of elasticity for 40 PPI polyurethane foam is approximately 7×10^6 N/m^2. If the rms pressure fluctuations are on the order of 0.01q, where q is the dynamic pressure $\left[\frac{1}{2}\rho U_\infty^2\right]$, a one dimensional steady-state estimation of the elastic substrate deformation is given by

$$\Delta a = \frac{0.01q\ T_s}{E} \tag{19}$$

Using Walters' data, the maximum displacement of the membrane allowed by the substrate would be on the order of 10^{-3}mm, which indicates that $\Delta a/\delta_{B.L.}$ is less than 10^{-5}. On the other hand, if a gap was present and Schlichting's (Ref. 34) roughness criterion is used as a crude estimate of the maximum amplitude,

$$\Delta a = 100\ \frac{\nu}{U_\infty} \tag{20}$$

By this criterion, a gap of up to 0.1 mm could be tolerated without inducing a roughness drag effect. In fact, a gap would appear to be necessary in order to produce a large enough amplitude fluctuation to affect the flow. How the estimated amplitude reported here and the data of Figure 5 are related cannot be determined until membrane surface displacements are actually measured.

The work of Mattout (Ref. 2) adds a new dimension to the compliant wall effect. Mattout's passive compliant wall experiments in water were inconclusive. The present theory indicates that his difficulty resulted from membrane vibration frequencies which were too high relative to his turbulent pressure spectrum as shown in Figure 4. However Mattout found the rather startling result that when the passive compliant surface was replaced by an active surface in which a traveling wave was mechanically generated at the membrane surface, it was possible in some cases to produce a thrust (in one case 5.29 times larger than the original skin friction drag). The effect of the mechanical wave device could easily have been to simultaneously control the frequency and amplitude of the compliant surface oscillations as well as supply the energy necessary for effective interaction.

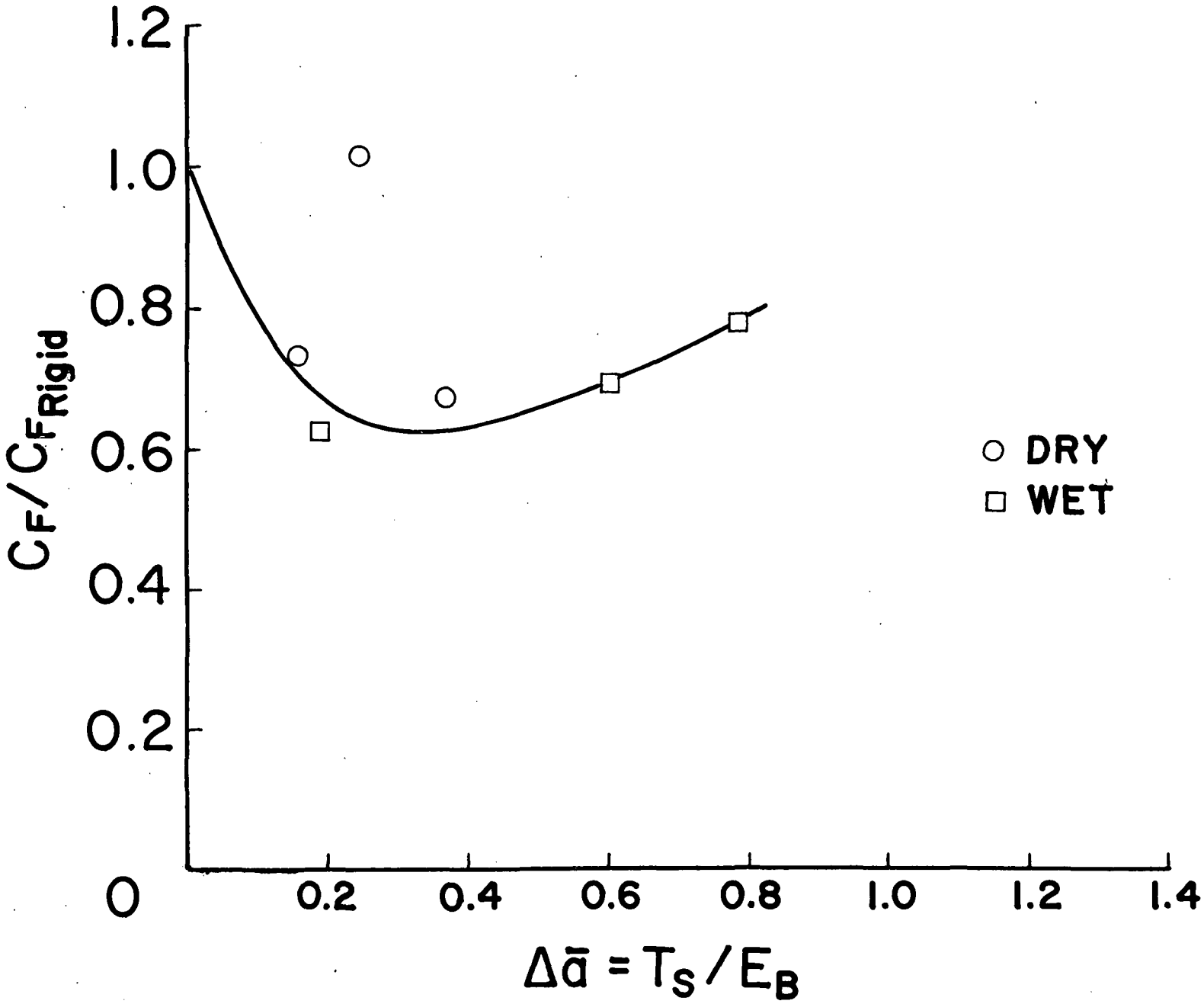

Figure 5. Influence of Blick's amplitude parameter on skin friction coefficient.

Boundary layer thickness measurements were not reported by Mattout. However, using his total length Reynolds numbers, his average turbulent boundary layer should have been approximately 3.7 cm thick when the water tunnel velocity was 1.5 m/sec. He employed an active surface 1 meter long and achieved his thrust effect when the wave speed was 8 times the tunnel velocity (12m/sec) in either direction. The amplitude of the wave oscillation was 1 mm or approximately 6% of the boundary layer thickness and the wave length was 52.5 cm. Using these data, the frequency of the surface wave was 22.9 Hz which is equivalent to a Strouhal number ($2\pi f\delta_{B.L.}/U_\infty$) of 3.55.

The other active wall data reported by Mattout had wave frequencies which were characterized by lower Strouhal numbers. Furthermore, the considerably more modest skin friction reduction produced by his other active wall experiments fall into the band of possible compliant drag reduction shown in Figure 4.

The author suggests that the thrust achieved by Mattout could have produced either of two effects consistent with the present theory. (1) A resonance effect may have occurred in which the wall motion was able to effectively stop the rigid wall streak shedding-Reynolds stress generation process in a manner similar to the relaminarization mechanism in rotating flows discussed by Kline, Reynolds, Schraub and Runstadler (Ref. 29) and replace it with the undulating wall, negative Reynolds stress generation process. (2) Or alternatively, the wall motion may have caused massive bursting of high and low speed streaks in a manner where the high speed streaks dominated the local Reynolds stresses--thereby causing locally negative Reynolds stresses as suggested by Grass (Ref. 31). In either case, the more modest drag reductions (still as high as 27%) induced mechanically by the wave generating equipment seem to agree with the compliant wall idea that energy must be withdrawn from the turbulent flow in order to cause a drag reduction. That is, the mechanical energy supplied to achieve drag reduction by the wave mechanism was in fact an alternate energy supply which produced the same effect as when the compliant wall removed energy from the high frequency portion of the energy containing eddies. The reason that such small drag reductions were achieved by Mattout in his passive wall experiments was due to a lack of energy available in the very high frequencies required to initiate impulse like membrane response, (his vibration frequencies were too high relative to the peak in the energy spectrum).

CONCLUSIONS

The author has concluded that compliant wall drag reduction in turbulent boundary layer flow is probably caused by a controlled panel flutter surface motion. A membrane surface can be excited by turbulent pressure fluctuations resulting from the higher frequency energy containing eddies, and lower frequency surface motions can produce locally negative Reynolds stresses either by a positive $u'v'$ correlation or by ejection of high velocity streaks. The magnitude of overall drag reduction depends upon the characteristic vibration frequencies of the membrane surface and the amplitude of the membrane motion, which both must be controlled. The vibration frequency can be controlled by the membrane dimensions, material properties and applied tensions. The amplitude can be controlled by the same membrane parameters as well as by properties and dimensions of the backing material and the spacing between the membrane and its backing. The theory is closely linked with the bursting model developed by the Stanford group and expanded by Grass. It is based on the hypothesis that a primary cause of streak shedding is the interaction between low speed streaks and incident high velocity eddies, as well as the assumption that streak shedding is primarily responsible for Reynolds stress and turbulent energy production. Only under these conditions are the active wall experiments reported by Mattout consistent with the proposed compliant wall mechanism.

In order to verify the proposed theory, detailed studies of the turbulent near wall flow structure over a compliant wall are needed as well as measurements of the amplitude and frequency of motion exhibited by a successful drag reducing surface. An experimental study of the frequency and amplitude characteristics of low-speed drag reducing surfaces similar to Blick's is currently underway at the National Bureau of Standards in Washington, D. C. The Fluid Mechanics Branch at Langley Research Center is currently engaged in similar experiments at much higher airspeeds.

APPENDIX A

RESPONSE OF A NON-UNIFORMLY LOADED RECTANGULAR MEMBRANE TO UNSTEADY PRESSURE FORCES

In general, a rectangular membrane subjected to aerodynamic forces can be represented as shown in Figure A-1. If the airflow is in the $\bar{x}$-direction and the membrane is under tension in the $\bar{y}$-direction, the applied loads would be $T_x(\bar{x})$ and T_y where T_x and T_y are the tension forces in the x- and y-directions respectively. It is important to realize that $T_x(\bar{x})$ varies with x due to the drag force acting in the direction of flow.

If $\bar{z}$ is the local vertical membrane displacement and it is assumed that unsteady translational motions of the membrane are negligible, the membrane displacement is governed by:

$$\frac{\partial}{\partial \bar{x}}\left(T_x \frac{\partial \bar{z}}{\partial \bar{x}}\right) + T_y \frac{\partial^2 \bar{z}}{\partial \bar{y}^2} + \bar{p} = \rho h \frac{\partial^2 \bar{z}}{\partial \bar{t}^2} \qquad \text{(A-1)}$$

where $\bar{p}$, ρ and h are the local pressure, membrane density, and membrane thickness, respectively.

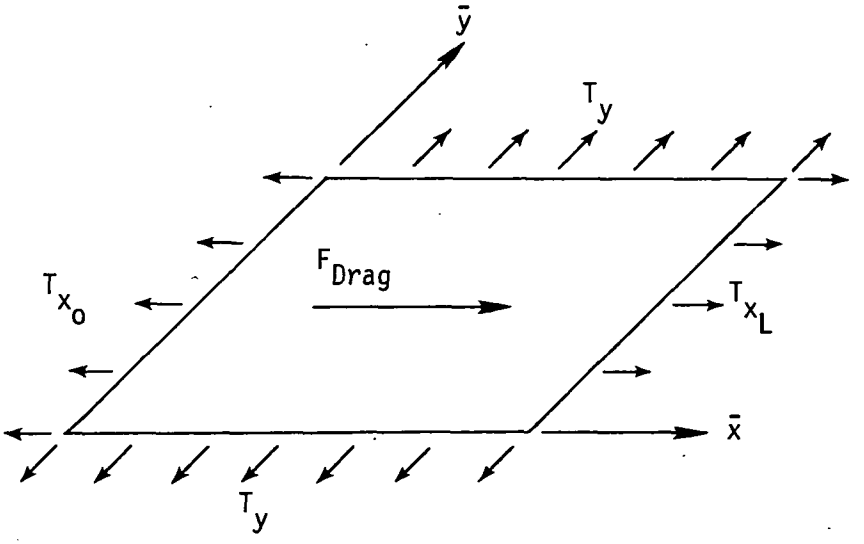

Figure A-1. Drag Forces Acting on a Rectangular Membrane.

If it is assumed that the membrane is initially flat and motionless, and that it is rigidly anchored at its edges, the appropriate initial and boundary conditions are:

$$\bar{z}(\bar{x},\bar{y},o) = \frac{\partial \bar{z}}{\partial \bar{t}}(\bar{x},\bar{y},o) = 0 \tag{A-2}$$

and

$$\bar{z}(o,\bar{y},\bar{t}) = \bar{z}(\bar{x},o,\bar{t}) = \bar{z}(L,\bar{y},\bar{t}) = \bar{z}(\bar{x},w,\bar{t}) = 0 \tag{A-3}$$

where it is assumed that the membrane length in the $\bar{x}$-direction is L and its width in the $\bar{y}$-direction is W.

At this point, a particular form for $T_x(\bar{x})$ is needed. As a reasonable and simple approximation, it is convenient to assume that the local drag shear stress is a constant and that the applied tension varies linearly with location in the x-direction. Hence, $T_x(\bar{x})$ is given by:

$$T_x(\bar{x}) = T_{x_o}\left[1 - \frac{f_D \bar{x}}{L}\right] \tag{A-4}$$

where

$$f_D \equiv \frac{F_{Drag}}{T_{x_o} W} \tag{A-5}$$

At this point dimensionless variables can be introduced into the system of equations. Let

$$x = \frac{\bar{x}}{L},\ y = \frac{\bar{y}}{L},\ \text{and}\ z = \frac{\bar{z}}{h}$$

while

$$t = \bar{t}\sqrt{T_{x_o}/(\rho L^2 h)},\ p = \bar{p}L^2/(T_{x_o} h), \tag{A-6}$$

and

$$\Theta(x) = T_x(x)/T_{x_o}$$

Then, the system of equations governing the motion of a rectangular membrane can be written:

$$\frac{\partial}{\partial x}\Theta\frac{\partial z}{\partial x} + \gamma\frac{\partial^2 z}{\partial y^2} + p = \frac{\partial^2 z}{\partial t^2} \tag{A-7}$$

where

$$\gamma = T_y/T_{x_o}$$

subject to:

$$z(x,y,o) = \frac{\partial z}{\partial t}(x,y,o) = 0 \tag{A-8}$$

and

$$z(o,y,t) = z(1,y,t) = z(x,o,t) = z(x,\beta,t) = 0 \tag{A-9}$$

where

$$\beta = w/L.$$

From the dimensionless formulation, it can be seen that the motion of the membrane is affected by the dimensionless parameters $\alpha = T_y/T_{x_o}$, $\beta = W/L$ and $f_D = F_{Drag}/T_{x_o}W$.

By substituting the functional form for $\theta(x)$ into (A-7) the governing equation can be written:

$$\frac{\partial}{\partial x}\left[(1 - f_D x)\frac{\partial z}{\partial x}\right] + \gamma \frac{\partial^2 z}{\partial y^2} = \frac{\partial^2 z}{\partial t^2} - p \tag{A-10}$$

That equation can be solved by classical transform methods.

Taking the Laplace transform of the governing equation and boundary conditions, while simultaneously employing the initial conditions, (A-10) becomes:

$$\frac{\partial}{\partial x}\left[(1 - f_D x)\frac{\partial \zeta}{\partial x}\right] + \gamma \frac{\partial^2 \zeta}{\partial y^2} + \Pi = s^2 \zeta \tag{A-11}$$

where

$$\zeta \equiv \int_0^\infty e^{-st}\, z(x,y,t)\, dt \tag{A-12}$$

and

$$\Pi \equiv \int_0^\infty e^{-st}\, p(x,y,t)\, dt \tag{A-13}$$

The transformed boundary conditions are:

$$\zeta(o,y) = \zeta(1,y) = \zeta(x,o) = \zeta(x,\beta) = 0 \tag{A-14}$$

Taking the finite Fourier sine transform of the equation, we get:

$$\frac{d}{dx}\left[(1 - f_D x)\frac{d\zeta_m}{dx}\right] - \frac{m^2\pi^2}{\beta^2}\gamma\zeta_m + \Pi_m = s^2\zeta_m \tag{A-15}$$

where

$$\zeta_m \equiv \int_0^\beta \zeta(x,y) \sin\frac{m\pi y}{\beta}\, dy \tag{A-16}$$

and

$$\Pi_m \equiv \int_0^\beta \Pi(x,y) \sin\frac{m\pi y}{\beta}\, dy \tag{A-17}$$

In order to complete the development, it is necessary to modify the form of $\frac{d}{dx}\left[(1 - f_D x)\frac{dw}{dx}\right]$ by employing a coordinate transformation. Let

$$\eta^2 = 1 - f_D x \tag{A-18}$$

Then

$$\frac{d\eta}{dx} = \frac{-f_D}{2\eta}$$

and

$$(1 - f_D x)\frac{dw}{dx} = -\frac{f_D \eta}{2}\frac{dw}{d\eta}$$

while

$$\frac{d}{dx}\left[(1 - f_D x)\frac{dw}{dx}\right] = \frac{f_D^2}{4}\eta\frac{d}{d\eta}\left(\eta\frac{dw}{d\eta}\right)$$

If the boundary conditions are at x = 0 and x = 1--say

$$w(o) = w(1) = 0,$$

the corresponding values of η are:

$$\eta = 1 \text{ at } x = 0$$

and

$$\eta = \sqrt{1 - f_D} \text{ at } x = 1$$

Now equations in the form

$$\frac{1}{\eta}\frac{d}{d\eta}\left(\eta\frac{dw}{d\eta}\right) + \frac{4\Gamma^2}{f_D^2}w = 0 \tag{A-19}$$

have the solution:

$$w(\eta) = AJ_o(\lambda\eta) + BY_o(\lambda\eta) \tag{A-20}$$

where

$$\lambda = \frac{2r}{f_D}$$

Applying the boundary conditions yields:

$$w_j(\eta) = Y_o(\lambda_j\kappa)J_o(\lambda_j\eta) - J_o(\lambda_j\kappa)Y_o(\lambda_j\eta) \tag{A-21}$$

where λ_j is the "jth" zero of:

$$Y_o(\lambda_j\kappa)J_o(\lambda_j) - J_o(\lambda j\kappa)Y_o(\lambda_j) = 0 \tag{A-22}$$

and

$$\kappa = \sqrt{1 - f_D}$$

A finite Hankel transform can now be employed to complete the solution of (A-15). First, the x-coordinate is replaced by η, given by (A-18). Then, the governing equation becomes:

$$\frac{f_D^2}{4}\frac{1}{\eta}\frac{d}{d\eta}\left(\eta\frac{d\zeta_m}{d\eta}\right)\eta - \frac{m^2\pi^2}{\beta^2}\gamma\zeta_m + \Pi_m = s^2\zeta_m \tag{A-23}$$

Next, the equation is multiplied by $\eta N_j(\eta)$ where:

$$N_j(\eta) \equiv Y_o(\gamma_j\kappa)J_o(\lambda_j\eta) - J_o(\lambda_j\kappa)Y_o(\lambda_j\eta) \tag{A-24}$$

and integrated between $\eta = \sqrt{1 - f_D}$ and $\eta = 1$, which yields:

$$\frac{-f_D^2}{4}\lambda_j^2\zeta_{mj} - \frac{m^2\pi^2}{\beta^2}\gamma\zeta_{mj} + \Pi_{mj} = s^2\zeta_{mj}$$

or

$$\zeta_{mj} = \frac{\Pi_{mj}}{s^2 + \frac{m^2\pi^2}{\beta^2} + \frac{f_D^2\lambda_j^2}{4}} \tag{A-25}$$

where

$$\zeta_{mj} \equiv \int_\kappa^1 \eta N_j(\eta)\zeta_m d\eta$$

and

$$\Pi_{mj} \equiv \int_\kappa^1 \eta N_j \Pi_m d\eta \tag{A-26}$$

The inversion of equation (A-25) is given by:

$$z(x,y,t) = L^{-1}\left\{\sum_{m=1}^{\infty}\sum_{n=1}^{\infty}\frac{\zeta_{mj}N_j(\eta)\sin\frac{m\pi y}{\beta}}{||Nj||^2 \cdot ||\sin\frac{m\pi y}{\beta}||^2}\right\} \quad \text{(A-27)}$$

where

$$||\sin\frac{m\pi y}{\beta}||^2 = \int_0^{\beta}\sin^2\frac{m\pi y}{\beta}\,dy = \frac{\beta}{2} \quad \text{(A-28)}$$

and

$$||N_j||^2 = \int_{\kappa}^{1}\eta N_j^2(\eta)\,d\eta \quad \text{(A-29)}$$

$$= \frac{Y_0(\lambda_j\kappa)\,J_1(\lambda_j) - \kappa^2 J_1(\lambda_j\kappa) - J_0(\lambda_j\kappa)\,Y_1(\lambda_j) - \kappa^2 Y_1(\lambda_j\kappa)}{2}$$

Response to a Unit Impulse Function

Since all pressure fluctuations can be constructed from a local impulse solution, it is only necessary to investigate the pressure field:

$$p(x,y,t) = \delta(x - x_0)\delta(y - y_0)\delta(t - t_0) \quad \text{(A-30)}$$

where δ is the unit impulse function. For this condition,

$$\Pi = \delta(x - x_0)\delta(y - y_0)\,e^{-st_0}$$

$$\Pi_m = \delta(x - x_0)\sin\frac{m\pi y_0}{\beta}\,e^{-st_0}$$

and

$$\Pi_{mj} = N_j(\sqrt{1 - f_D x_0})\,\sin\frac{m\pi y_0}{\beta}\,e^{-st_0} \quad \text{(A-31)}$$

Consequently,

$$\zeta_{mi} = \frac{N_j(\sqrt{1 - f_D x_0})\,\sin\frac{m\pi y_0}{\beta}\,e^{-st_0}}{s^2 + \frac{m^2\pi^2}{\beta^2} + \frac{f_D^2\lambda_j^2}{4}} \quad \text{(A-32)}$$

and

$$\text{if} \quad \eta_0 = \sqrt{1 - f_D x_0}\ ,$$

$$z(x,y,t) = \frac{4}{\beta} \sum_{m=1}^{\infty} \sum_{j=1}^{\infty} \frac{N_j(\eta_o)N_j(\eta) \sin \frac{m\pi y_o}{\beta} \sin \frac{m\pi y}{\beta} \sin \Gamma_{mj}(t - t_o)}{\Gamma_{mj}\left\{Y_o(\lambda_j\kappa)[J_1(\lambda_j) - \kappa^2 J_1(\lambda_j\kappa)] - J_o(\lambda_j\kappa)[Y_1(\lambda_j) - \kappa^2 Y_1(\lambda_j\kappa)]\right\}} \tag{A-33}$$

where

$$\Gamma_{mj}^2 = \frac{m\pi}{\beta}^2 + \frac{f_D\lambda_j}{2}^2 \tag{A-34}$$

In order to evaluate this solution, it is necessary to determine the dimensionless parameters characterizing Blick's (Ref. 19) data. For reference purposes, the following equations have been used:

$$\beta = w/L = 0.1825 \tag{A-35}$$

$$T_{x_o} = T_x + \frac{F_{Drag}}{W} = T_x + 0.594\ C_f \tag{A-36}$$

$$f_D = F_{Drag}/WT_{x_o} = 0.4125/\left[0.594 + (T_x/C_f)\right] \tag{A-37}$$

A computer program has been written to determine the response of membranes of the type used by Blick. However, the drag force effect has been found negligibly small in the case of Blick's experiments.

APPENDIX B

RESPONSE OF A TWO-DIMENSIONAL ELASTIC SLAB TO HARMONIC PRESSURE FLUCTUATIONS*

Neglecting body forces, the conservation of momentum equations for a two-dimensional slab can be written:

$$\rho\frac{\partial^2 u}{\partial t^2} = \frac{\partial \tau_{xy}}{\partial y} + \frac{\partial \sigma_x}{\partial x} \tag{B-1}$$

and

$$\rho\frac{\partial^2 v}{\partial t^2} = \frac{\partial \tau_{yx}}{\partial x} + \frac{\partial \sigma_y}{\partial y} , \tag{B-2}$$

where ρ is the density of the slab material, u and v are the horizontal and vertical displacements, respectively, of a point in the slab, while σ_x, σ_y and τ_{xy} are the normal horizontal stress, normal vertical stress, and shear stress, respectively.

If the slab is perfectly elastic, the stresses are related to strains by:

$$\tau_{xy} = \tau_{yk} = G\left(\frac{\partial u}{\partial y} + \frac{\partial v}{\partial x}\right) \tag{B-3}$$

$$\sigma_x = \lambda\left(\frac{\partial u}{\partial x} + \frac{\partial v}{\partial y}\right) + 2G\frac{\partial u}{\partial x} \tag{B-4}$$

and

$$\sigma_y = \lambda\left(\frac{\partial u}{\partial x} + \frac{\partial v}{\partial y}\right) + 2G\frac{\partial v}{\partial y} , \tag{B-5}$$

where λ and G are constants describing the particular material, and are discussed further at the end of this appendix.

If the front surface of the slab is exposed to a moving, periodic stress field, σ_y and τ_{xy} can be represented at the surface by:

$$\sigma_y(x,o,t) = G\omega\, R_e\left\{e^{i\alpha(x-ct)}\right\} \tag{B-6}$$

---

*Based on the work of Nonweiler (Ref. 10)

and

$$\tau_{xy}(x,o,t) = G\tau\, R_e\left\{e^{i\alpha(x-ct)}\right\} \tag{B-7}$$

where $R_e\{\ \}$ is defined as the real part of $\{\ \}$. Hence, the complex functions of X and Y must satisfy the stress boundary conditions:

$$\left[\lambda\left(\frac{\partial X}{\partial x} + \frac{\partial Y}{\partial y}\right) + 2G\frac{\partial Y}{\partial y}\right]_{y=o} = G\omega e^{i\alpha(x-ct)} \tag{B-8}$$

and

$$\left[G\left(\frac{\partial X}{\partial y} + \frac{\partial Y}{\partial x}\right)\right]_{y=o} = G\tau e^{i\alpha(x-ct)} \tag{B-9}$$

where

$$u = R_e\{X\} \text{ and } v = R_e\{Y\} \tag{B-10}$$

The real parts of X and Y must satisfy the conservation of momentum equations (B-1) and (B-2). By assuming X and Y obey the same conservation of momentum equations as u and v, they are governed by:

$$\lambda\left(\frac{\partial^2 X}{\partial x^2} + \frac{\partial^2 Y}{\partial x \partial y}\right) + 2G\frac{\partial^2 X}{\partial x^2} + G\frac{\partial^2 X}{\partial y^2} + G\frac{\partial^2 Y}{\partial y \partial x} = \rho\frac{\partial^2 X}{\partial t^2} \tag{B-11}$$

and

$$\lambda\left(\frac{\partial^2 Y}{\partial y^2} + \frac{\partial^2 X}{\partial x \partial y}\right) + 2G\frac{\partial^2 Y}{\partial y^2} + G\frac{\partial^2 X}{\partial x \partial y} + G\frac{\partial^2 Y}{\partial x^2} = \rho\frac{\partial^2 Y}{\partial t^2} \tag{B-12}$$

If the front surface of the slab is exposed continuously to a harmonic stress field, it is reasonable to assume that the deformations of the slab will follow similar harmonic paths. That is, X and Y should take the form:

$$X(x,y,t) = f(y)e^{i\alpha(x-ct)} \tag{B-13}$$

and

$$Y(x,y,t) = g(y)e^{i\alpha(x-ct)} \tag{B-14}$$

Substituting these functional forms into equations (B-11) and (B-12), f and g are governed by:

$$\lambda(-\alpha^2 f + i\alpha g') - 2G\alpha^2 f + Gf'' + i\alpha Gg' = -\rho\alpha^2 c^2 f \tag{B-15}$$

and

$$\lambda(i\alpha f' + g'') + 2Gf'' + i\alpha Gf' - \alpha^2 Gg = -\rho\alpha^2 c^2 g \tag{B-16}$$

Or, rearranging:

$$(\rho\alpha^2c^2 - \lambda\alpha^2 - 2G\alpha^2)f + Gf'' = -i\alpha(G + \lambda)g'$$

and

$$(\rho\alpha^2c^2 - \alpha^2G)g + (2G + \lambda)g'' = -i\alpha(G + \lambda)f'$$

Defining constants C_1 and C_2 by:

$$C_1^2 = (\lambda + 2G)/\rho \text{ and } C_2^2 = G/\rho \tag{B-17}$$

the governing equations of f and g can be written:

$$\alpha^2(\rho C^2 - \rho C_1^2)f + \rho C_2^2 f'' = -i\alpha\rho(C_1^2 - C_1^2)g' \tag{B-18}$$

$$\alpha^2(\rho C^2 - \rho C_2^2)g + \rho C_1^2 g'' = -i\alpha\rho(C_1^2 - C_2^2)f' \tag{B-19}$$

Finally, defining r_1 and r_2 by:

$$r_1^2 = 1 - \left(\frac{C}{C_1}\right)^2 \quad \text{and} \quad r_2^2 = 1 - \left(\frac{C}{C_2}\right)^2 \tag{B-20}$$

and letting coordinate η be defined:

$$\eta = \alpha y \tag{B-21}$$

The governing equations (B-18) and (B-19) can be rewritten:

$$f_{\eta\eta} - \left(\frac{C_1}{C_2}\right)^2 r_1^2 f = -i\left[\left(\frac{C_1}{C_2}\right)^2 r_1^2 - r_2^2\right] g_\eta \tag{B-22}$$

and

$$g_{\eta\eta} - \left(\frac{C_2}{C_1}\right)^2 r_2^2 g = -i\left[r_1^2 - \left(\frac{C_2}{C_1}\right) r_2^2\right] f_\eta \tag{B-23}$$

These equations can be combined by differentiating (B-22) with respect to η and rewriting (B-23) as:

$$f_\eta = \frac{g_{\eta\eta} - \left(\frac{C_2}{C_1}\right)^2 r_2^2 g}{-i\left[r_1^2 - \left(\frac{C_2}{C_1}\right)^2 r_2^2\right]} \tag{B-24}$$

Then, the combined governing equation becomes:

$$\frac{d^4g}{d\eta^4} + \left[\left(\frac{C_2}{C_1}\right)^2 (r_2^2 - 1)r_2^2 + \left(\frac{C_1}{C_2}\right)^2 (r_1^2 - 1)r_1^2 - 2r_1^2 r_2^2\right] \frac{d^2g}{d\eta^2} + r_1^2 r_2^2 g$$

$$= -\left[r_1^2 - \left(\frac{C_2}{C_1}\right)^2 r_2^2\right]\left[\left(\frac{C_1}{C_2}\right)^2 r_1^2 - r_2^2\right] \frac{d^2g}{d\eta^2}$$

Or, defining D by:

$$D = \frac{d}{d\eta} \tag{B-25}$$

and rearranging:

$$\left\{D^4 + \left[\left(\frac{C_2}{C_1}\right)^2 (r_2^2 - 1)r_2^2 + \left(\frac{C_1}{C_2}\right)^2 (r_1^2 - 1)r_1^2 - 2r_1^2 r_2^2\right] D^2 - 2r_1^2 r_2^2 \right\} g = 0$$

But

$$\left(\frac{C_2}{C_1}\right)^2 (r_2^2 - 1)r_2^2 = \frac{1-r_1^2}{1-r_2^2} (r_2^2 - 1)r_2^2 = (r_1^2 - 1)r_2^2$$

and

$$\left(\frac{C_1}{C_2}\right)^2 (r_1^2 - 1)r_1^2 = (r_2^2 - 1)r_1^2$$

Therefore, the governing equation can be written:

$$\left[D^4 - (r_1^2 + r_2^2)D^2 + r_1^2 r_2^2\right] g = 0$$

or

$$(D + r_1)(D - r_1)(D + r_2)(D - r_2)\, g = 0 \tag{B-26}$$

The general solution to this equation can be written:

$$g(\eta) = a_1 \cosh r_1\eta + a_2 \sinh r_1\eta + a_3 \cosh r_2\eta + a_4 \sinh r_2\eta \tag{B-27}$$

The solution for $g(\eta)$ can be used in (B-24) to solve for $f(\eta)$. That is,

$$\frac{df}{d\eta} = i \frac{\frac{d^2g}{d\eta^2} - \left(\frac{C_2}{C_1}\right)^2 r_2^2 g}{r_1^2 - \left(\frac{C_2}{C_1}\right)^2 r_2^2} = i \frac{(r_2^2 - 1)\frac{d^2g}{d\eta^2} - (r_1^2 - 1)r_2^2 g}{r_2^2 - r_1^2} \tag{B-28}$$

Substituting in (B-26) and simplifying,

$$\frac{df}{d\eta} = i\left[a_1 \cosh r_1\eta + a_2 \sinh r_1\eta + r_2^2(a_3 \cosh r_2\eta + a_4 \sinh r_2\eta)\right] \tag{B-29}$$

Integrating,

$$f(\eta) = i\left[\frac{a_1}{r_1}\sinh r_1\eta + \frac{a_2}{r_1}\cosh r_1\eta + r_2 a_3 \sinh r_2\eta + r_2 a_4 \cosh r_2\eta\right] \tag{B-30}$$

If new constants A_1, A_2, A_3 and A_4 are defined by:

$$A_1 = i\alpha a_1\ ,\quad A_2 = i\alpha r_2 a_4\ ,\quad A_3 = i\alpha\frac{a_2}{r_1}\ \text{and}\ A_4 = i\alpha a_3\ , \tag{B-31}$$

then $f(\eta)$ and $g(\eta)$ are given by:

$$f(\eta) = \frac{A_1}{\alpha r_1}\sinh r_1\eta + \frac{A_3}{\alpha}\cosh r_1\eta + A_4 \sinh r_2\eta + \frac{A_2}{\alpha}\cosh r_2\eta \tag{B-32}$$

and

$$g(\eta) = \frac{A_1}{i\alpha}\cosh r_1\eta + \frac{r_1 A_3}{i\alpha}\sinh r_1\eta + \frac{A_4}{i\alpha}\cosh r_2\eta + \frac{A_2}{i\alpha r_2}\sinh r_2\eta \tag{B-33}$$

Consequently, the complex solutions X and Y are given by:

$$X(x,\eta,t) = \frac{1}{\alpha}\left[\frac{A_1}{r_1}\sinh r_1\eta + A_3\cosh r_1\eta + r_2 A_4 \sinh r_2\eta + A_2 \cosh r_2\eta\right] e^{i\alpha(x-ct)} \tag{B-34}$$

$$Y(x,\eta,t) = \frac{1}{i\alpha}\left[A_1 \cosh r_1\eta + r_1 A_3 \sinh r_1\eta + A_4 \cosh r_2\eta + \frac{A_2}{r_2}\sinh r_2\eta\right] e^{i\alpha(x-ct)} \tag{B-35}$$

Applying the front surface boundary conditions (B-8) and (B-9),

$$\frac{\lambda}{G}\left[i(A_3 + A_2) - i(r_1^2 A_3 + A_2)\right] - 2i(r_1^2 A_3 + A_2) = \omega$$

or

$$\left[\left(\frac{\lambda + 2G}{G}\right) r_1^2 - \frac{\lambda}{G}\right] A_3 + 2A_2 = i\omega \tag{B-36}$$

and

$$(A_1 + r_2^2 A_4) + (A_1 + A_4) = \tau\ ,$$

or

$$2A_1 + (1 + r_2^2)A_4 = \tau \tag{B-37}$$

Employing the definitions of r_1, r_2, C_1 and C_2, equation (B-36) can be rewritten:

$$2A_2 + (1 + r_2^2)\, A_3 = i\omega \tag{B-38}$$

The remaining boundary conditions can be developed by assuming that the back surface of the slab is motionless. Then,

$$u(x, -D,t) = v(x, -D,t) = 0 \tag{B-39}$$

And because of the form of $X(x,\eta,t)$, $Y(x,\eta,t)$, these conditions require that:

$$\frac{-A_1}{r_1} \sinh r_1 d + A_3 \cosh r_1 d - r_2 A_4 \sinh r_2 d + A_2 \cosh r_2 d = 0 \tag{B-40}$$

and

$$A_1 \cosh r_1 d - r_1 A_3 \sinh r_1 d + A_4 \cosh r_2 d - \frac{A_2}{r_2} \sinh r_2 d = 0 \tag{B-41}$$

where $d = \alpha D$.

The boundary condition requirements on the integration constants can be written in matrix form as:

$$\begin{bmatrix} 2 & 0 & 0 & (1 + r_2^2) \\ 0 & 2 & (1 + r_2^2) & 0 \\ \dfrac{-\sinh r_1 d}{r_1} & \cosh r_2 d & \cosh r_1 d & -r_2 \sinh r_2 d \\ \cosh r_1 d & \dfrac{-\sinh r_2 d}{r_2} & -r_1 \sinh r_1 d & \cosh r_2 d \end{bmatrix} \begin{bmatrix} A_1 \\ A_2 \\ A_3 \\ A_4 \end{bmatrix} = \begin{bmatrix} \tau \\ i\omega \\ 0 \\ 0 \end{bmatrix} \tag{B-42}$$

Alternatively, the front surface conditions can be used to write

$$\begin{aligned} A_4 &= \frac{\tau}{1 + r_2^2} - \frac{2}{1 + r_2^2} A_2 \\ A_3 &= \frac{i\omega}{1 + r_2^2} - \frac{2}{1 + r_2^2} A_1 \end{aligned} \tag{B-43}$$

and the back surface boundary conditions can be used to generate the 2 x 2 matrix equation:

$$\begin{bmatrix} -\beta_{11} & \beta_{12} \\ \beta_{21} & -\beta_{22} \end{bmatrix} \begin{bmatrix} A_1 \\ A_2 \end{bmatrix} = \begin{bmatrix} \gamma_1 \\ \gamma_2 \end{bmatrix} \tag{B-44}$$

where,

$$\beta_{11} = \frac{1 + r_2^2}{r_1} \sinh r_1 d + r \cosh r_1 d \tag{B-45}$$

$$\beta_{12} = (1 + r_2^2) \cosh r_2 d + 2r_2 \sinh r_2 d \tag{B-46}$$

$$\beta_{21} = (1 + r_2^2) \cosh r_1 d + 2r_1 \sinh r_1 d \tag{B-47}$$

$$\beta_{22} = \frac{1 + r_2^2}{r^2} \sinh r_2 d + 2 \cosh r_2 d \tag{B-48}$$

$$\gamma_1 = \tau r_2 \sinh r_2 d - i\omega \cosh r_2 d \tag{B-49}$$

and

$$\gamma_i = i\omega r_1 \sinh r_1 d - T \cosh r_2 d \tag{B-50}$$

Solving equation (B-44) and employing relations (B-43), the constants of integration are given by:

$$A_1 = \frac{\beta_{22} \gamma_1 + \beta_{12} \gamma_2}{\beta_{12} \beta_{21} - \beta_{11} \beta_{22}} \tag{B-51}$$

$$A_2 = \frac{\beta_{21} \gamma_1 + \beta_{11} \gamma_2}{\beta_{12} \beta_{21} - \beta_{11} \beta_{22}} \tag{B-52}$$

$$A_3 = \frac{i\omega(\beta_{12} \beta_{21} - \beta_{11} \beta_{22}) - 2(\beta_{22}\gamma_1 + \beta_{12}\gamma_2)}{(1 + r_2^2)(\beta_{12}\beta^{21} - \beta_{11}\beta_{22})} \tag{B-53}$$

$$A_4 = \frac{\tau(\beta_{12} \beta_{21} - \beta_{11} \beta_{22}) - 2(\beta_{21} \gamma_1 + \beta_{11} \gamma_2)}{(1 + r_2^2)(\beta_{12} \beta_{21} - \beta_{11} \beta_{22})} \tag{B-54}$$

Now γ_1 and γ_2 have real and imaginary parts. As a result, all of the integration constants are complex and can be written:

$$A_n = A_n^R + iA_n^I \tag{B-55}$$

Specifically,

$$A_1^R = \frac{\tau r_2 \beta_{22} \sinh r_2 d - \tau \beta_{12} \cosh r_2 d}{\beta_{12} \beta_{21} - \beta_{11} \beta_{22}} \tag{B-56}$$

$$A_1^I = \frac{\omega r_1 \beta_{12} \sinh r_1 d - \omega \beta_{22} \cosh r_1 d}{\beta_{12} \beta_{21} - \beta_{11} \beta_{22}}$$

$$A_2^R = \frac{\tau r_2 \beta_{21} \sinh r_2 d - \tau \beta_{11} \cosh r_2 d}{\beta_{12} \beta_{21} - \beta_{11} \beta_{22}} \tag{B-57}$$

$$A_2^I = \frac{\omega r_1 \beta_{11} \sinh r_1 d - \omega \beta_{21} \cosh r_1 d}{\beta_{12} \beta_{21} - \beta_{11} \beta_{22}}$$

$$A_3^R = \frac{2\tau\beta_{12} \cosh r_2 d - 2\tau r_2 \beta_{22} \sinh r^2 d}{(1 + r_2^2)(\beta_{12} \beta_{21} - \beta_{11} \beta_{22})} \tag{B-58}$$

$$A_3^I = \frac{2\omega(\beta_{22} \cosh r_1 d - r_1 \beta_{12} \sinh r_1 d)}{(1 + r_2^2)(\beta_{12} \beta_{21} - \beta_{11} \beta_{22})} + \frac{\omega}{1 + r_2^2}$$

$$A_4^R = \frac{2\tau(\beta_{11} \cosh r_2 d - r_2 \beta_{21} \sinh r_2 d)}{(1 + r_2^2)(\beta_{12} \beta_{21} - \beta_{11} \beta_{22})} + \frac{\tau}{1 + r_2^2} \tag{B-59}$$

and

$$A_4^I = \frac{2\omega(\beta_{21} \cosh r_1 d - r_1 \beta_{11} \sinh r_1 d)}{(1 + r_2^2)(\beta_{12} \beta_{21} - \beta_{11} \beta_{22})}$$

Consequently, the local displacements are given by:

$$\begin{aligned} u(x,\eta,t) = R_e\{X(x,\eta,t)\} = \frac{1}{\alpha}\Bigg[& \frac{A_1^R}{r_1} \sinh r_1\eta + A_3^R \cosh r_1\eta \\ & + r_2 A_4^R \sinh r_2\eta + A_2^R \cosh r_2\eta \Bigg] \cos \alpha(x-ct) \\ & + \frac{-1}{\alpha}\Bigg[\frac{A_1^I}{r_1} \sinh r_1\eta + A_3^I \cosh r_1\eta + r_2 A_4^I \sinh r_2\eta \\ & + A_2^I \cosh r_2\eta \Bigg] \sin \alpha(x-ct) \end{aligned} \tag{B-60}$$

$$\begin{aligned} v(x,\eta,t) = R_e\, Y(x,\eta,t) = \frac{1}{\alpha}\Bigg[& A_1^R \cosh r_1\eta + r_1 A_3^R \sinh r_1\eta \\ & + A_4^R \cosh r_2\eta + \frac{A_2^R}{r_2} \sinh r_2\eta \Bigg] \sin \alpha(x-ct) \\ & + \frac{1}{\alpha}\Bigg[A_1^I \cosh r_1\eta + r_1 A_3^I \sinh r_1\eta + A_4^I \cosh r_2\eta \\ & + \frac{A_2^I}{r_2} \sinh r_2\eta \Bigg] \cos \alpha(x-ct) \end{aligned} \tag{B-61}$$

The motion of the front surface is then given by:

$$u(x,o,t) = \frac{1}{\alpha}\left[(A_3{}^R + A_4{}^R)\cos\alpha(x-ct) - (A_3{}^I + A_2{}^I)\sin\alpha(x-ct)\right] \tag{B-62}$$

$$v(x,o,t) = \frac{1}{\alpha}\left[(A_1{}^R + A_4{}^R)\sin\alpha(x-ct) + (A_1{}^I + A_4{}^I)\cos\alpha(x-ct)\right] \tag{B-63}$$

Accordingly, the maximum vertical displacement is given by:

$$v_{max} = \frac{1}{\alpha}\left[(A_1{}^R + A_4{}^R)^2 + (A_1{}^I + A_4{}^I)^2\right]^{1/2} \tag{B-64}$$

Application of this solution to representative compliant materials is currently under investigation.

As a final point of reference, the constants G and λ which have been used to describe the elastic material are related to the modulus of elasticity (E) and Poisson's ratio (ν) by:

$$\lambda = \nu E \quad \text{and} \quad G = \frac{1-\nu}{2}E \tag{B-65}$$

A foam whose modulus of elasticity is 10 psi and Poisson's ratio is 0.3 would have constants

$$\lambda = 432 \text{ psf} \quad \text{and} \quad G = 504 \text{ psf}.$$

REFERENCES

1. Blick, E. F.; Walters, R. R.; Smith, R. and Chu, H. H. "Compliant Coating Skin-Friction Experiments," AIAA Paper No. 69-165, 1969.
2. Mattout, R.: "Réduction de trainée par parois souples" ("Reduction of Drag by Flexible Walls"),Association Technique Maritime et Aeronautique, Bulletin, No. 72, pp 207-227, 1972.
3. Kramer, M. O.: "Boundary Layer Stabilization by Distributed Damping", J. Aeronaut. Sci., Vol. 27, pp 68-76; Also J. Am. Soc. Nav. Eng., Vol. 72, pp 25-33, 1960.
4. Kramer, M. O.: "The Dolphin's Secret", J. Am. Soc. Nav. Eng., Vol. 73, pp 103-107, 1961.
5. Benjamin, T. B.: "Effects of a Flexible Boundary on Hydrodynamic Stability", J. Fluid Mech., Vol. 9, pp 513-532, 1960.
6. Benjamin, T. B.: "The Threefold Classification of Unstable Disturbances in Flexible Surfaces Bounding Inviscid Flows", J. Fluid Mech., Vol. 16, pp 436-450, 1963.
7. Benjamin, T. B.: "Fluid Flow with Flexible Boundaries", in Applied Mechanics: Proceedings of the Eleventh International Congress of Applied Mechanics (Munich, Germany) 1964, edited by H. Görtler, Springer-Verlag, Berlin, pp 109-127, 1966.
8. Kaplan, R. E.: "The Stability of Laminar Incompressible Boundary Layers in the Presence of Compliant Boundaries" Mass. Inst. Tech. Aeroelasticity and Structures Research Laboratory Report No. 116-1, 1964.
9. Landahl, M. T.: "On the Stability of a Laminar Incompressible Boundary Layer Over a Flexible Surface", J. Fluid Mech., Vol. 13, pp 609-631, 1962.
10. Nonweiler, T.: "Qualitative Solution of the Stability Equation for a Boundary Layer in Contact with Various Forms of a Flexible Surface," Aero. Res. Council Report C-P. 622, 1963.
11. Gyorgyfalvy, D.: "Possibilities of Drag Reduction by Use of a Flexible Skin", J. Aircraft, Vol. 4, No. 3, pp 186-192, 1967.
12. Laufer, J. and Maestrello, L.: "The Turbulent Boundary Layer Over a Flexible Surface", Boeing Co., Transportation Div., Document D6-9708, 1965.

13. Ritter, H. and Porteous, J. S., "Water Tunnel Measurements of Skin Friction on a Compliant Coating", Admiralty Research Laboratory Report A.R.L. /N3/6/HY/9/7, A.R.L. /6/N8. 1965.
14. Dinkelacker, A., "Preliminary Experiments on the Influence of Flexible Walls on Boundary Layer Turbulence", Deutsche Luftund Raumfahrt, Forschungebercht 66-78; Also J. Sound Vibr., Vol. 4, pp. 187-214, 1966.
15. Karplus, H. B.; "Turbulent Flow Transition Near Solid and Flexible Boundarys", Ill. Inst. Tech. Research Inst., Report No. IITRI 1205-4, 1963.
16. Fisher, D. H. and Blick, E. F.; "Turbulent Damping by Flabby Skins", J. Aircraft, Vol. 3, No. 2, pp. 163-164, 1966.
17. Blick, E. F. and Looney, W. R.; "Skin Friction Coefficients on Compliant Surfaces in Turbulent Flow", J. Spacecraft and Rockets, Vol. 3, No. 10, pp 1562-1564, 1966.
18. Looney, W. R.; "Skin Friction Coefficients of Compliant Surfaces in Turbulent Flow", M. E. Thesis, Univ. of Okla., 1966.
19. Blick, E. F.; Bert, C. W.; Reed, T. D.; Walter, R. R.; and Wares, R. N.; "Aerodynamic Drag Reduction Using Compliant Coatings", Proc. Okla. Acad. Sci., Vol. 47, pp. 429-440, 1966.
20. Blick, E. F. and Walters, R. R.; "Turbulent Boundary Layer Characteristics of Compliant Surfaces", J. Aircraft, Vol. 5, No. 1, pp 11-16, 1968.
21. Smith, R. L. and Blick, E. F., "Skin Friction of Compliant Surfaces with Foamed Material Substrate", J. Hydronautics, Vol. 3, No. 2, pp 100-102, 1969.
22. Chu, H. H.; "Drag Characteristics for a Compliant Surface Airfoil", Ph.D. Dissertation, Univ. of Okla., 1969.
23. Lissaman, P.B.S. and Harris, G. L.; "Turbulent Skin Friction on Compliant Surfaces", AIAA Paper No. 69-164, 1969.
24. Ffowcs-Williams, J. E.; "Reynolds Stress Near a Flexible Surface Responding to an Unsteady Flow", Bolt, Beranek and Newman, Inc., Report No. 1138, 1964.
25. Blick, E. F.; "The Theory of Skin Friction Reduction by a Compliant Coating in a Turbulent Boundary Layer", in Viscous Drag Reduction, Plenum Press, New York, 1969.

26. Semenov, B. N.; "Interaction of an Elastic Boundary with the Viscous Sublayer of a Turbulent Boundary Layer", NASA Technical Translation TTF-14,391, from Zhurnal Prikladnoy Mekhaniki i Tekhnicheskoy Fiziki, May-June, No. 3, pp 58-62, 1971.

27. Vaicaitis, R.; "Generalized Random Forces for Rectangular Panels", AIAA Journal, Vol. 11, No. 7, pp 984-988, 1973.

28. Walters, R. R.; "Turbulent Boundary Layer Characteristics of Flow Over A Compliant Surface", Ph.D. Dissertation, Univ. of Okla., 1969.

29. Kline, S.J.: Reynolds, W. C.; Schraub, F. A. and Runstadler, P. W.; "The Structure of Turbulent Boundary Layers", J. Fluid Mech., Vol. 30, pp 741-773, 1967.

30. Kim, H. T.; Kline, S. J. and Reynolds, W. C.; "The Production of Turbulence Near a Smooth Wall in a Turbulent Boundary Layer", J. Fluid Mech., Vol. 50, pp 133-160, 1971.

31. Grass, A. J.; "Structural Features of Turbulent Flow Over Smooth and Rough Boundaries", J. Fluid Mech., Vol. 50, pp 233-255, 1971.

32. Bradshaw, P.; "An Introduction to Turbulence and its Measurement", Pergamon Press, Oxford, pg. 32, 1971.

33. Bull, M. K.; "Wall-Pressure Fluctuation Associated with Subsonic Turbulent Boundary Layer Flow", J. Fluid Mech., Vol. 28, pp 719-754, 1967.

34. Schlichting, H.; Boundary-Layer Theory, 6th Edition, McGraw-Hill, New York, pg. 618. 1968.

NATIONAL AERONAUTICS AND SPACE ADMINISTRATION
WASHINGTON, D.C. 20546

OFFICIAL BUSINESS
PENALTY FOR PRIVATE USE $300

SPECIAL FOURTH-CLASS RATE BOOK

POSTAGE AND FEES PAID
NATIONAL AERONAUTICS AND SPACE ADMINISTRATION
451

U.S.MAIL

POSTMASTER: If Undeliverable (Section 158 Postal Manual) Do Not Return

"The aeronautical and space activities of the United States shall be conducted so as to contribute . . . to the expansion of human knowledge of phenomena in the atmosphere and space. The Administration shall provide for the widest practicable and appropriate dissemination of information concerning its activities and the results thereof."

—NATIONAL AERONAUTICS AND SPACE ACT OF 1958

NASA SCIENTIFIC AND TECHNICAL PUBLICATIONS

TECHNICAL REPORTS: Scientific and technical information considered important, complete, and a lasting contribution to existing knowledge.

TECHNICAL NOTES: Information less broad in scope but nevertheless of importance as a contribution to existing knowledge.

TECHNICAL MEMORANDUMS: Information receiving limited distribution because of preliminary data, security classification, or other reasons. Also includes conference proceedings with either limited or unlimited distribution.

CONTRACTOR REPORTS: Scientific and technical information generated under a NASA contract or grant and considered an important contribution to existing knowledge.

TECHNICAL TRANSLATIONS: Information published in a foreign language considered to merit NASA distribution in English.

SPECIAL PUBLICATIONS: Information derived from or of value to NASA activities. Publications include final reports of major projects, monographs, data compilations, handbooks, sourcebooks, and special bibliographies.

TECHNOLOGY UTILIZATION PUBLICATIONS: Information on technology used by NASA that may be of particular interest in commercial and other non-aerospace applications. Publications include Tech Briefs, Technology Utilization Reports and Technology Surveys.

Details on the availability of these publications may be obtained from:

SCIENTIFIC AND TECHNICAL INFORMATION OFFICE

NATIONAL AERONAUTICS AND SPACE ADMINISTRATION

Washington, D.C. 20546